

Geophysical Research Letters[®]

RESEARCH LETTER

10.1029/2023GL108028

Distribution of Seed Electron Phase Space Density Minima in Earth's Radiation Belts



Key Points:

- The deepening Phase Space Density (PSD) minima are noticeably observed at $\mu < 300$ MeV/G, with occurrence reaching 15%
- The simulation can produce deepening PSD minima at $\mu < 60$ MeV/G
- The modeled seed electron deepening PSD minima are influenced by L -dependent electron lifetimes due to interaction with hiss waves

Supporting Information:

Supporting Information may be found in the online version of this article.

Correspondence to:

A. Y. Drozdov,
adrozdov@ucla.edu

Citation:





Drozdov, A. Y., Allison, H. J., Saikin, A. A., Schiller, Q., & Wang, D. (2024). Distribution of seed electron phase space density minima in Earth's radiation belts. *Geophysical Research Letters*, *51*, e2023GL108028. <https://doi.org/10.1029/2023GL108028>

Received 6 JAN 2024

Accepted 11 MAR 2024

Author Contributions:

Conceptualization: A. Y. Drozdov
Data curation: A. Y. Drozdov
Formal analysis: A. Y. Drozdov
Funding acquisition: A. Y. Drozdov, A. A. Saikin
Methodology: A. Y. Drozdov, H. J. Allison, A. A. Saikin, Q. Schiller
Project administration: A. Y. Drozdov
Visualization: A. Y. Drozdov
Writing – original draft: A. Y. Drozdov
Writing – review & editing: A. Y. Drozdov, H. J. Allison, A. A. Saikin, Q. Schiller, D. Wang

A. Y. Drozdov¹ , H. J. Allison² , A. A. Saikin¹ , Q. Schiller³ , and D. Wang² 

¹University of California Los Angeles, Los Angeles, CA, USA, ²GFZ German Centre for Geosciences, Potsdam, Germany, ³Space Science Innovations, Greenbelt, MD, USA

Abstract We conducted a statistical analysis of local phase space density (PSD) minima across a wide energy range (~ 20 keVs to ~ 10 MeV), using observations from the Van Allen Probes and the Geostationary Operational Environmental Satellite. We identified deepening minima in PSD profiles of multi-MeV ($\sim 5\%$ occurrence) and of “seed” electrons (up to 15% occurrence, corresponding to ~ 70 – 100 s keV) and compared their distribution with a 3D diffusion model using the Versatile Electron Radiation Belts (VERB) code. The comparison of the observed and modeled distributions suggests that the PSD minima of seed electrons are likely associated with hiss waves and the corresponding L -shell dependent electron lifetimes. However, the observed distribution was not fully reproduced by the model, potentially indicating other fast loss mechanisms of seed electrons.

Plain Language Summary This study presents a comprehensive analysis of the behavior of electrons within the Earth's radiation belts, specifically focusing on changes in the phase space density (PSD) across various energy levels. By analyzing data from the Van Allen Probes and the GOES satellite over 4 years, we observed notable reductions in PSD, particularly at very high-energy electrons and somewhat lower energy electrons, often referred to as “seed” electrons. These reductions or minima in PSD are important for understanding the dynamics within the radiation belts. The study found that these minima can be explained by interactions with certain types of waves in space, like electromagnetic ion cyclotron or hiss waves. Furthermore, the PSD minima of the seed electrons likely depend on variations in the rate at which hiss waves can scatter electrons at various distances.

1. Introduction

The analysis of phase space density (PSD) L -shell (or L^*) profiles constructed at fixed first and second adiabatic invariants is crucial for the investigation of the radiation belt dynamics, as these profiles serve as key indicators of the acceleration and loss mechanisms at play (e.g., Allison & Shprits, 2020; Boyd et al., 2018; Green & Kivelson, 2004; Iles et al., 2006; Zhao et al., 2019). The acceleration due to the inward radial diffusion results in radial monotonic PSD profiles (Baker et al., 2014; Chen et al., 2006; Olfier et al., 2021), while the local acceleration events are accompanied by growing PSD peaks (Allison et al., 2021; Li et al., 2014; Reeves et al., 2013; Thorne et al., 2013). The outward radial diffusion and magnetopause shadowing effect (e.g., Turner, Shprits, et al., 2012) are effective loss mechanisms also identifiable in PSD profiles with a distinct negative gradient at the outer boundary of the radiation belts (Shprits et al., 2006; Staples et al., 2022; Turner, Angelopoulos, et al., 2012; Wu et al., 2020). Wave-particle interactions can produce localized loss, such as precipitation into the atmosphere (e.g., Millan & Thorne, 2007; Shprits et al., 2008). This precipitation can occur as a slow process, leading to a gradual decrease in PSD, or as a fast localized interaction, resulting in deepening PSD minima (Shprits et al., 2017).

One of the mechanisms leading to fast localized loss is electromagnetic ion cyclotron (EMIC) waves (Bingley et al., 2019; Summers & Thorne, 2003; Usanova et al., 2014), which in conjunction with chorus and hiss waves play a defining role in the dynamics of multi-MeV radiation belt electrons (Bashir et al., 2021; Drozdov et al., 2020). However, EMIC waves are ineffective in scattering of sub-MeV electrons and require special conditions such as: high background plasma density, high parallel to background magnetic field wave vector, and/or high wave power at the proximity of the upper cutoff gyrofrequency (Denton et al., 2019; Ukhorskiy et al., 2010). While the calculation of minimum resonant energy typically relies on cold plasma, EMIC waves primarily contribute to the loss of $>MeV$ electrons, even under hot plasma approximation (e.g., Bashir

© 2024. The Authors.

This is an open access article under the terms of the [Creative Commons Attribution License](https://creativecommons.org/licenses/by/4.0/), which permits use, distribution and reproduction in any medium, provided the original work is properly cited.

et al., 2022; Cao et al., 2017). Such wave-particle interaction results in a distinct EMIC waves signature, characterized by PSD minima, which has been observed in many studies (Blum et al., 2020; Bruno et al., 2022; Da Silva et al., 2021; Drozdov et al., 2017; Kim et al., 2021; Ma et al., 2020; Shprits et al., 2016; Xiang et al., 2017; Xiong et al., 2021). However, the PSD minima were also observed at energies that correspond to sub-MeV (Capannolo et al., 2019; Yan et al., 2023) suggesting that EMIC waves can also contribute to the loss of those electrons (Hendry et al., 2019, 2021; Rodger et al., 2015). Nevertheless, it remains unclear how often PSD minima are detected at low energies and what mechanisms are responsible for the rapid depletion of sub-MeV electrons.

Drozdov et al. (2022) conducted a statistical study on the deepening PSD minima and reported that the depletion of multi-MeV electrons is in good agreement with the EMIC wave activity. However, the study was limited to 1 year of observations (1 October 2012–1 October 2013) and focused on analyzing PSD minima within the energy range of $\mu \in [1,000, 5,500]$ MeV/G (corresponding to \sim MeV to multi-MeV). This paper presents a follow-up study in which we investigate PSD deepening minima over an extended period, including 4 years of observations and an extended energy range, including “seed” electrons (\sim 20 keV–100 s keV).

2. Data

We used Van Allen Probes A and B's combined pitch-angle resolved electron flux data product (Boyd et al., 2021) based on the Energetic Particle, Composition and Thermal Plasma Suite (RBSP-ECT) instrument (Spence et al., 2013). This cross-calibrated data set consists of three-minute-averaged flux spectra spanning a broad energy range (from 15 eV to 20 MeV). In addition, we used flux measured by GOES-15 satellite which is equipped with the Energetic Proton, Electron, and Alpha particle Detector (EPEAD) and the Magnetospheric Electron Detector, providing measurements from \sim 30 keV electrons up to $>$ 2 MeV. We calculated adiabatic invariants and equatorial pitch angles using the T89 magnetic field model (Tsyganenko, 1989) with the International Geomagnetic Reference Field internal magnetic field models. The measured flux was subsequently converted into PSD as described in the following section.

3. Methodology

3.1. PSD Calculation

To convert from flux to PSD, we followed the methodology described by Drozdov et al. (2022). This process involves binning using median values on each orbital pass on the grid of μ , K , and L^* . However, whereas our previous study (Drozdov et al., 2022) covered 1 year and range μ (1,000–5,500 MeV/G), here we expand the temporal and spectral coverage to include 4 years (2013–2017) and given the broad energy range provided by RBSP-ECT data set we extended to cover three orders of magnitude of μ . Specifically, μ has a range of (10–10,000 MeV/G) in 28 irregular bins: 10–100 MeV/G with the step of 10 MeV/G, 100–1,000 MeV/G with the step of 100 MeV/G, and 1,000–10,000 MeV/G with the step of 1,000 MeV/G. Furthermore, to eliminate any noisy outliers present within the PSD data, we applied a moving average local regression smoothing filter that assigns lower weight to outliers with a first-degree polynomial model (using Matlab function “smooth” with “rlowess” method).

For reference, the binning in K and L^* were the same as in Drozdov et al. (2022): 10 bins of K , 0.001 – $1 G^{1/2} R_E$, with variable step: $K \in [10^{-4}, 3 \cdot 10^{-4}, 7 \cdot 10^{-4}, 10^{-3} \dots 1] G^{1/2} R_E$, and 21 bins of L^* , 3.5 – 5.5 , with the step of 0.1 . The PSD profiles were extended to high L^* using GOES measurements, which are close to Van Allen Probes measurements thus eliminating the need for intercalibration (Baker et al., 2019). The profiles are interpolated along L^* , and normalized to perform the search of PSD minima.

3.2. PSD Minima Identification

We used the same minimum identification method as in Drozdov et al. (2022), briefly summarized here. First, we identified local minima on a normalized PSD L^* profile for each orbital pass, and each value of μ and K . Then we discarded the minima that did not match the following criterias: (a) the ratio threshold (between local minimum and the minimal nearest local maximum) is ≥ 1.2 ; (b) a minimum of two points below the threshold; (c) the PSD value at the minimum is at least 10% lower than on the previous available orbital pass (within 9 hr) to ensure that the minimum is likely a result of the loss.

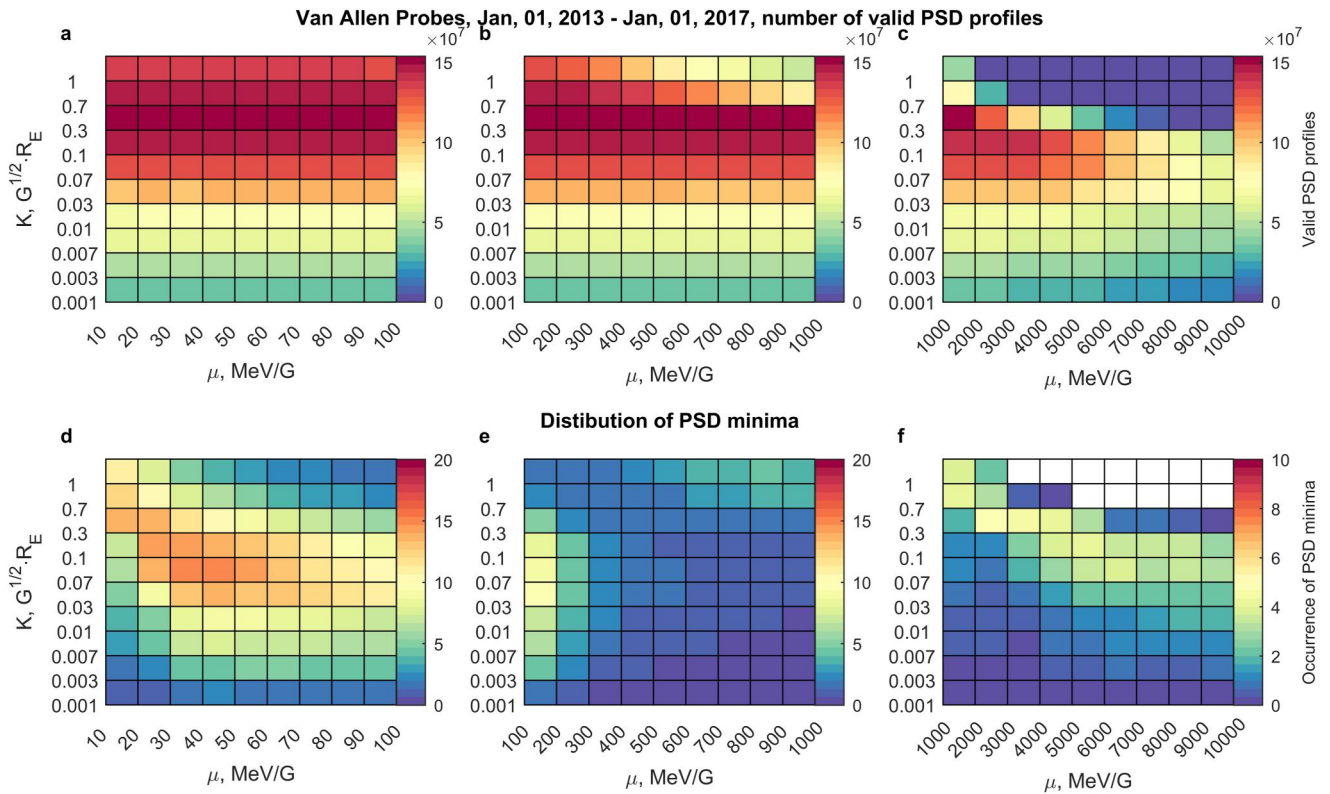


Figure 1. (a–c) Number of valid phase space density (PSD) profiles. (d–f) Occurrence of PSD minima as a function of μ and K . The columns correspond to different μ range: (a, d) $\mu \in [10, 100]$ MeV/G; (b, e) $\mu \in [100, 1,000]$ MeV/G; (c, f) $\mu \in [1,000, 10,000]$ MeV/G; (d–f) the different color bar ranges are selected to emphasize the shape of the distributions.

3.3. VERB Simulations

To compare the observed results with the modeling, we used the same long-term simulation setup as in Drozdov et al. (2022). We used the Versatile Electrons Radiation belts (VERB) code to solve the Fokker-Planck equation on a single grid of modified adiabatic invariants (Subbotin & Shprits, 2012). The simulation included activity-dependent K_p -driven hiss and chorus (Spasojevic et al., 2015; Zhu et al., 2019) waves, Carpenter and Anderson (1992) plasmopause model, lightning-generated whistler waves, and man-made transmitters-generate very low frequency (VLF) waves based on Subbotin et al. (2011). To be consistent with Drozdov et al. (2017), the EMIC waves were parameterized by solar wind dynamic pressure, and the initial and boundary conditions ($L^* = 5.5$) were driven by Van Allen Probe observations. These parameters were previously used in the VERB code simulations and showed good agreement with observations (see Drozdov et al., 2020, 2021; Zhu et al., 2019). The simulation time step was set at 1 hr. In addition to the above simulation, we performed a second simulation without hiss waves, but using a constant decay rate of $\tau = 10$ days inside the plasmopause (see Shprits et al., 2005) representing a simplified loss due to hiss waves scattering without L^* or energy dependence.

4. Results

4.1. Observed Distribution of PSD Minima

Panels a–c in Figure 1 show the total number of valid PSD profiles available between 1 January 2013 and 1 January 2017. Each column corresponds to the μ range of 10–100, 100–1,000, and 1,000–10,000 MeV/G, respectively. Panels d–f show the occurrence of identified PSD minima, which is presented as a percentage of available valid profiles (in panels a–c).

Figure 1f shows PSD minimum occurrence of multi-MeV electrons (1,000–10,000 MeV/G) which in quasi-linear theory have sufficient energy to interact with EMIC waves. Figure 1f indicates that 3%–5% of Van Allen Probe passes through the radiation belts observed PSD minima. The shape of the distribution indicates the interaction of

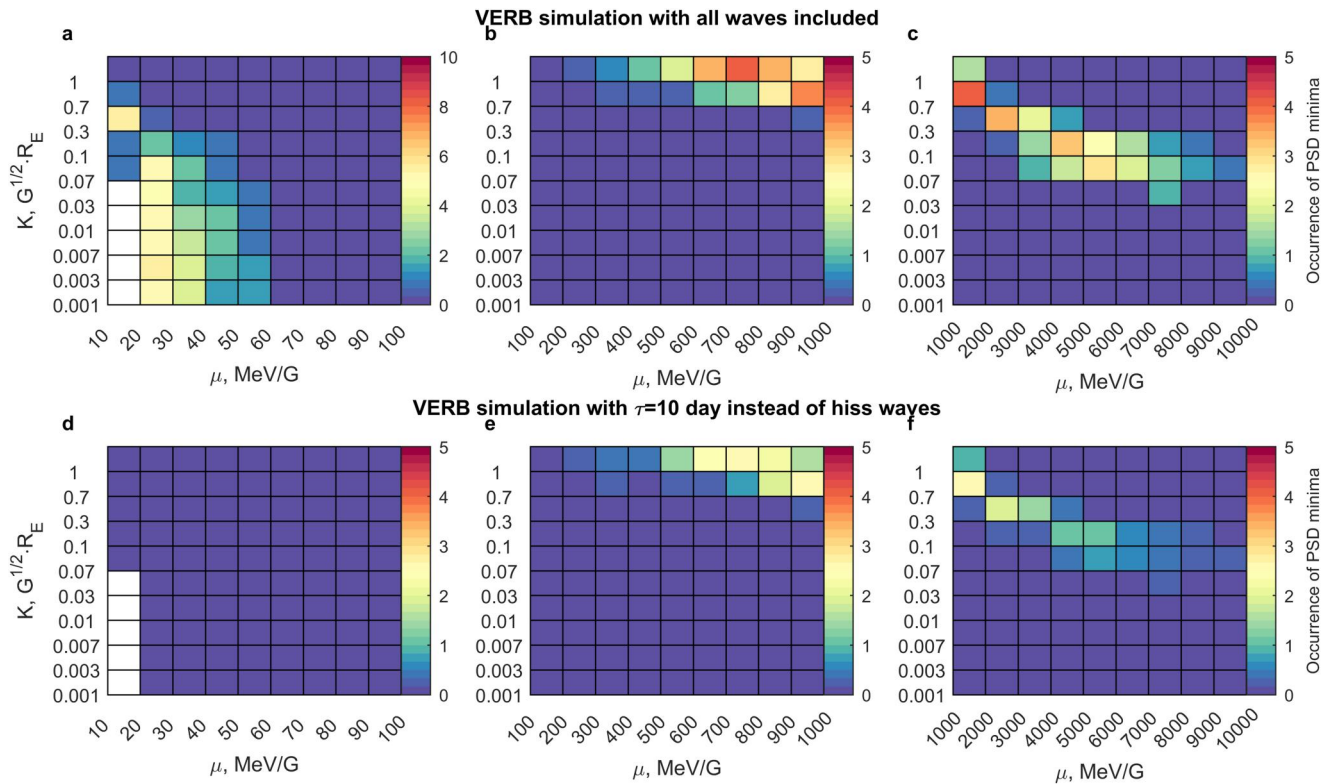


Figure 2. The distribution of phase space density minima as a function of μ and K is similar to Figure 1 but obtained from the Versatile Electron Radiation Belts code modeling. (a–c) Simulation with all waves included. (d–f) Simulation with hiss waves replaced with a constant decay rate of $\tau = 10$ days. The different color bar ranges are selected to emphasize the shape of the distributions.

those multi-MeV electrons with EMIC waves and confirms the conclusions of Drozdov et al. (2022) but based on a larger data set spanning 4 years. Figure 1e mostly corresponds to the electrons with energy from several hundred of keV up to a few MeV, indicating that the formation of the PSD minima in this energy range is not common. An interesting result is seen in Figure 1d, which represents seed electrons at lower energies (~ 20 – 100 keV) and shows that PSD minima occurrence can reach up to 12%–15% (note, the color bar's upper value is higher than in Figure 1f), spanning in a wide μ and K range. The distribution is maximized in the μ range of 20–60 MeV/G and in the K range of 0.03–0.3 $G^{1/2}R_E$ (which corresponds to approximately 70–500 keV). Notably, noticeable PSD minimum occurrence (up to 5%) is observed up to $\mu < 300$ MeV/G. Since the PSD minima were selected based on the consideration of deepening minima, this distribution indicates the presence of a fast localized loss process (on the timescale of a few hours). The observation of PSD minima is possible only when refilling the local PSD depletion due to the radial transport being slower than the localized loss process. Hence, we observe two distinct populations of electrons in the keV and multi-MeV ranges where PSD minima are noticeably observed, which suggests potentially different mechanisms of their formation. To better understand the processes responsible for the formation of the observed PSD minima distribution, we performed a long-term simulation using the VERB code to compare with these observations.

4.2. Long-Term Simulation Using VERB Code

Figure 2 shows the distribution of PSD minima obtained from long-term simulations, following the same methodology as for the processing of the observations. Figure 2 is presented in different color bar ranges to emphasize the shape of the distributions. However, since long-term simulations are computationally expensive, the simulations were limited to the period of 1 year of 2013, which overlapped with the observed period. We chose this year because it is representative of the 4-year period in the variety of geomagnetic and solar driving conditions. Note that we use simulations only to investigate the underlying processes that control the formation of

PSD minima. A full reproduction of the 4-year period requires an advanced simulation setup and will be a subject of future study.

Figure 2 is similar to Figures 1d–1f except that it analyzes the VERB simulation PSD profiles instead of those observed by the Van Allen Probes. The top row (panels a–c) illustrate the occurrence rate of PSD minima in the VERB simulation with all waves included (including the Zhu et al., 2019 hiss wave model), and the bottom row (panels d–f) show the occurrence rate in the VERB simulation substituting hiss waves inside the plasmasphere with a simple $\tau = 10$ days loss parameter for all μ/K . Notice that simulation (Figures 2b and 2c) indicates a similar shape and maximum of PSD minima occurrence as in observations at $\mu > 500$ MeV/G (Figures 1e and 1f). This result is expected as EMIC waves are included in the simulation. Note, that the loss of electrons is additionally aided by corresponding hiss, chorus, and VLF waves (see Drozdov et al., 2020). However, removing L^* and energy dependency from the hiss scattering rates affects the PSD minima formation at multi-MeV electrons and correspondingly prevents PSD minima formation at lower energies (Figure 2d). Figure 2a indicates the presence of the fast localized loss that leads to the formation of PSD minima at low energies ($\mu < 60$ MeV/G). However, the simulation did not fully reproduce the observed formation of PSD minima at μ up to 300 MeV/G (Figure 1d). Although the simulated distribution shows clear PSD deepening minima below $K \sim 0.3 G^{1/2} R_E$ and $\mu < 60$ MeV/G, the observed distribution is maximized at $\mu \sim 20$ –60 MeV/G and $K \sim 0.03$ – $0.3 G^{1/2} R_E$.

Hence, the simulation partially accounted for the loss processes responsible for the formation of PSD minima, but the comprehensive description of the observed phenomena is yet to be discovered. Nevertheless, the results of the similar simulation with constant decay rates instead of hiss waves (Figures 2d–2f) revealed the absence of PSD minima at $\mu < 300$ MeV/G, preserving the general distribution of PSD minima at multi-MeV energies (the shape of distribution in Figures 2b and 2c is similar to the on Figures 2e and 2f). This indicates that the accurate representation of the hiss waves and corresponding electron scattering rates is important in the formation of the PSD minima at low energies.

5. Discussion

To understand the formation mechanism of PSD minima at low μ we compared the time-dependent PSD profiles obtained from observations (Figure 3a) and VERB simulation (Figure 3b) with all waves included. In panels a and b, the crosses represent the L^* location of a PSD minimum, if present. Purple crosses are highlighted for detail in Figures 3c–3f. Figure 3a indicates sudden particle enhancements at low L shells (SPELLS) (Turner et al., 2017) that occurred on 1 March 2013, which led to a formation of the enhanced PSD at $L^* \sim 3.5$ followed by a gradual decay below the plasmopause location (red-white line, based on the Carpenter and Anderson (1992) model). Although, it may not seem obvious the local deepening PSD minima (crosses in Figure 3a) were formed after the SPELLS, which are clearly visible in Figures 3c–3f representing examples of observed normalized PSD profiles (corresponding purple crosses in Figure 3a). Examples of non-normalized PSD profiles are illustrated in Figure S1 in Supporting Information S1. The formed minima were located inside the plasmasphere where hiss waves are likely to be responsible for the local loss of the electrons. The VERB code simulation in Figure 3b shows the similar formation of SPELLS followed by the gradual decay of the electrons due to the hiss waves and corresponding deepening minima in PSD (red crosses). However, due to the diffusive nature of the simulation, the representation of PSD dynamics is more clear.

For reference, Figure 4 shows the L -shell and energy dependence of electron lifetimes (shown at $K_p = 4$) due to scattering by hiss waves (Zhu et al., 2019). The lifetimes are estimated based on the integral expression of the lowest pitch-angle diffusion timescale from Albert and Shprits (2009). Figure 3 demonstrates PSD minima during this period occurred in the L^* range of ~ 3.8 –4.2. According to Figure 4, at those L^* hiss waves can provide the fastest scattering of ~ 100 –150 keV electrons reaching the timescale of less than a day providing favorable conditions for the local minima formation. Note, in this L^* range the radial diffusion is in the timescale of days based on Brautigam and Albert (2000) parameterization, which can be also seen in the simulation (Figure 3b). Additionally, such energy dependence is aligned with the observed maximized distribution of PSD minima (μ range of 20–60 MeV/G, Figure 1a). However, since lifetimes shown in Figure 4 are calculated based on the average statistical model of the hiss waves and without accounting for the variation of geomagnetic activity, the realistic electron energy at which fast scattering is possible can vary. Figure 4 also shows that the lifetime is notably increasing with decreasing L -shell. This leads to the scenario when sudden enhancement of low energy

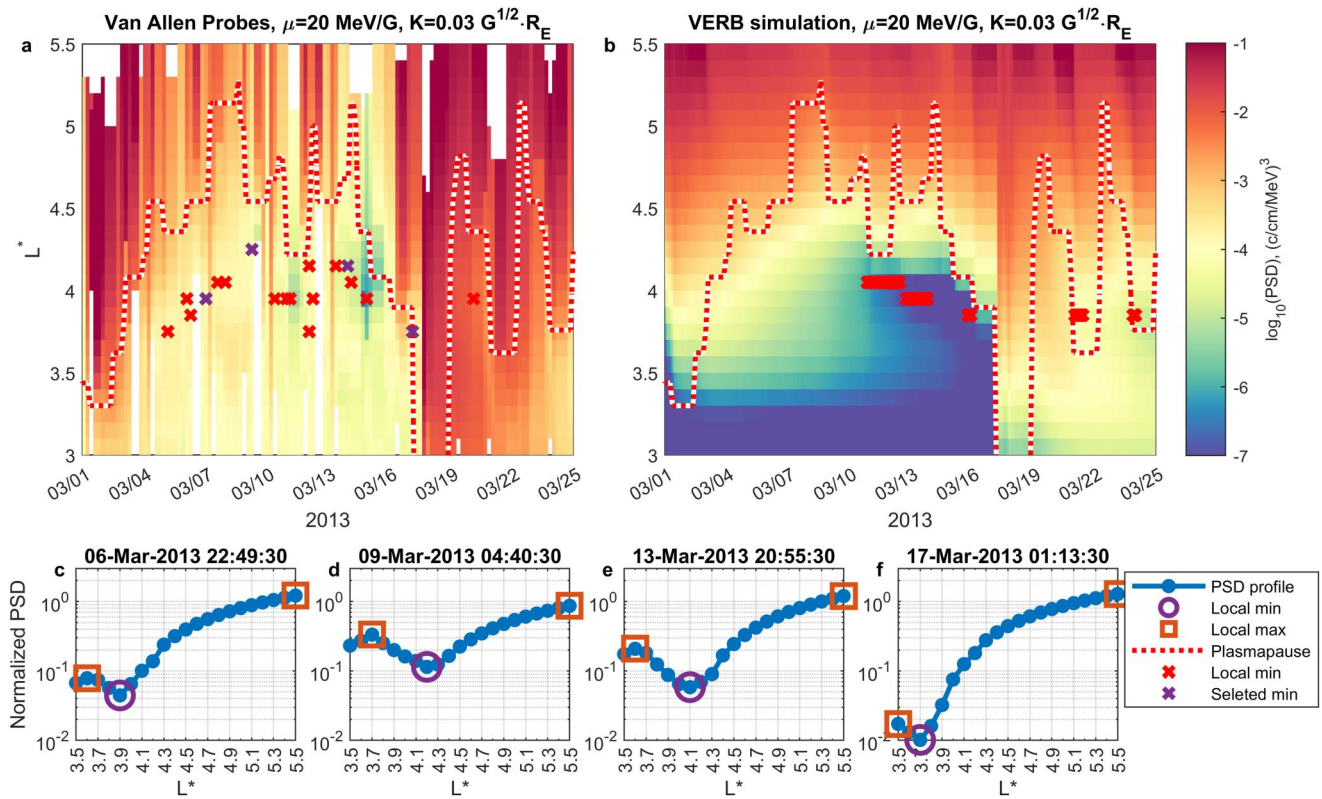


Figure 3. Observed (a) and modeled (b) Phase Space Density (PSD) profiles during March 2013. The white-red line indicates the location of the plasmapause (Carpenter & Anderson, 1992). The crosses (red or purple) indicate the locations of PSD deepening minima. Panels (c–f) show examples of observed normalized PSD profiles corresponding to the purple crosses in panel (a).

electrons at low L -shell ($L^* < 3.5$) can remain stable for some time (in a scale of days) while the electrons at higher L -shell, but inside the plasmasphere, experience sudden loss and a formation of the observed PSD minima.

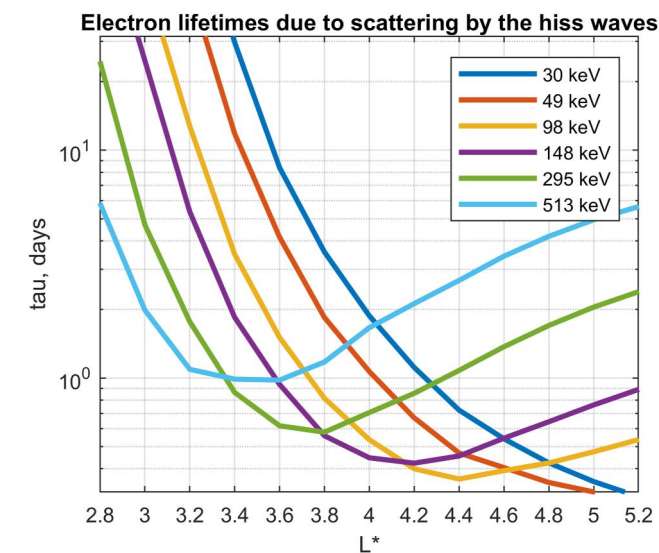


Figure 4. Electron lifetimes due to scattering by the hiss waves model (Zhu et al., 2019) at $K_p = 4$. Different line colors correspond to different energies, from 30 to 513 keV.

Furthermore, Figure S2 in Supporting Information S1 shows the PSD minima at $\mu \leq 300$ MeV/G are mainly located at -0.5 of plasmapause's L^* (Carpenter and Anderson, 1992), which corresponds to the location of the peak in hiss wave power (e.g., Malaspina et al., 2016). Conversely, PSD minima at $\mu \geq 500$ MeV/G are mainly aligned with the plasmapause location.

However, the other fast localized scattering processes may be responsible for the formation of the observed distribution of PSD minima. Convective transport is an important part of seed electron dynamics. Proper modeling of this population requires advanced simulation that includes convective transport using 4-D codes (e.g., Aseev et al., 2019; Haas et al., 2023; Shprits et al., 2015), which can change the dynamics of PSD minima formation. Other potentially important processes such as scattering by electron cyclotron harmonic waves, electron holes, and time domain structures (e.g., Fukuzawa et al., 2022; Horne et al., 2003; Mozer et al., 2017; Shen et al., 2021; Vasko et al., 2017). In addition, a further improvement to the simulation requires hiss waves parameterization by plasmapause location (Malaspina et al., 2018, 2020; Saikin et al., 2022). Finally, the choice of the magnetic field model can affect both observed and modeled distributions. However, sensitivity tests in previous case studies (e.g., Shprits et al., 2017, 2018) indicated that the magnetic field model did not play a significant role, at least in the case of EMIC-driven PSD minima formation. The inclusion of these factors will be the subject of future studies.

6. Conclusions

In this study, we conducted a statistical analysis of the electron radiation belt, focusing on the deepening of PSD minima across a broad range of first (μ) and second (K) adiabatic invariants. Using 4 years of Van Allen Probes and Geostationary Operational Environmental Satellite (GOES) measurements, we verified that the distribution of PSD deepening minima associated with multi-MeV electrons (μ ranging from 1,000 to 10,000 MeV/G) is consistent with losses due to interactions with EMIC wave activity, reaching the occurrence rate of 5%. This finding is consistent with the results obtained over a shorter 1-year period (Drozdov et al., 2022). Extended analysis of PSD profiles revealed frequent deepening minima for μ values below 300 MeV/G, indicative of seed electrons (tens to hundreds of keV). The occurrence of these PSD minima reaches up to 15% in the μ and K ranges, corresponding to energies approximately between 70 and 500 keV. This novel finding will be further explored in detail in future studies. Using VERB code modeling, we reproduced the presence of the PSD deepening minima at $\mu < 60$ MeV/G. We demonstrated that this distribution is likely influenced by hiss waves within the plasmasphere. Consequently, the distribution of seed electron PSD deepening minima may result from the variation in electron scattering rates across different L -shells. However, the observed distribution was not fully reproduced, potentially indicating the presence of additional fast localized seed electron scattering mechanisms.

Data Availability Statement

We thank the Van Allen Probe ECT team for providing the data (https://rbsp-ect.newmexicoconsortium.org/data_pub/). The GOES measurements are available at the NOAA NGDC website (<https://www.ncei.noaa.gov/data/goes-space-environment-monitor/access/full/>). The authors used geomagnetic indices provided by OMNIWeb (<https://omniweb.gsfc.nasa.gov/>). The data to reproduce the figures are available at UCLA dataverse repository (Drozdov, 2023).

Acknowledgments

This research is supported by NASA awards 80NSSC18K0663 and 80NSSC21K1693. This work used computational, and storage services associated with the Hoffman2 Shared Cluster provided by the UCLA Institute for Digital Research and Education's Research Technology Group. The authors also acknowledge the developers of the International Radiation Belt Environment Modeling (IRBEM) library. We thank Yuri Shprits, Alexander Boyd, and Drew Turner for the useful discussion.

References

- Albert, J. M., & Shprits, Y. Y. (2009). Estimates of lifetimes against pitch angle diffusion. *Journal of Atmospheric and Solar-Terrestrial Physics*, 71(16), 1647–1652. <https://doi.org/10.1016/j.jastp.2008.07.004>
- Allison, H. J., & Shprits, Y. Y. (2020). Local heating of radiation belt electrons to ultra-relativistic energies. *Nature Communications*, 11(1), 4533. <https://doi.org/10.1038/s41467-020-18053-z>
- Allison, H. J., Shprits, Y. Y., Zhelavskaya, I. S., Wang, D., & Smirnov, A. G. (2021). Gyroresonant wave-particle interactions with chorus waves during extreme depletions of plasma density in the Van Allen radiation belts. *Science Advances*, 7(5), eabc0380. <https://doi.org/10.1126/sciadv.abc0380>
- Aseev, N. A., Shprits, Y. Y., Wang, D., Wygant, J., Drozdov, A. Y., Kellerman, A. C., & Reeves, G. D. (2019). Transport and loss of ring current electrons inside geosynchronous orbit during the 17 March 2013 storm. *Journal of Geophysical Research Space Physics*, 124(2), 915–933. <https://doi.org/10.1029/2018JA026031>
- Baker, D. N., Jaynes, A. N., Li, X., Henderson, M. G., Kanekal, S. G., Reeves, G. D., et al. (2014). Gradual diffusion and punctuated phase space density enhancements of highly relativistic electrons: Van Allen Probes observations. *Geophysical Research Letters*, 41(5), 1351–1358. <https://doi.org/10.1002/2013GL058942>
- Baker, D. N., Zhao, H., Li, X., Kanekal, S. G., Jaynes, A. N., Kress, B. T., et al. (2019). Comparison of Van Allen probes energetic electron data with corresponding GOES-15 measurements: 2012–2018. *Journal of Geophysical Research Space Physics*, 124(12), 9924–9942. <https://doi.org/10.1029/2019JA027331>
- Bashir, M. F., Artemyev, A., Zhang, X., & Angelopoulos, V. (2021). Energetic electron precipitation driven by the combined effect of ULF, EMIC, and whistler waves. *Journal of Geophysical Research Space Physics*, 127(1), e2021JA029871. <https://doi.org/10.1029/2021ja029871>
- Bashir, M. F., Artemyev, A., Zhang, X.-J., & Angelopoulos, V. (2022). Hot plasma effects on electron resonant scattering by electromagnetic ion cyclotron waves. *Geophysical Research Letters*, 49(11), e2022GL099229. <https://doi.org/10.1029/2022gl099229>
- Bingley, L., Angelopoulos, V., Sibeck, D., Zhang, X., & Halford, A. (2019). The evolution of a pitch-angle “Bite-Out” scattering signature caused by EMIC wave activity: A case study. *Journal of Geophysical Research Space Physics*, 124(7), 5055–5065. <https://doi.org/10.1029/2018JA026292>
- Blum, L. W., Remya, B., Denton, M. H., & Schiller, Q. (2020). Persistent EMIC wave activity across the nightside inner magnetosphere. *Geophysical Research Letters*, 47(6), e2020GL087009. <https://doi.org/10.1029/2020gl087009>
- Boyd, A. J., Spence, H. E., Reeves, G. D., Funsten, H. O., Skoug, R. M., Larsen, B. A., et al. (2021). RBSP-ECT combined pitch angle resolved electron flux data product. *Journal of Geophysical Research Space Physics*, 126(3), e2020JA028637. <https://doi.org/10.1029/2020ja028637>
- Boyd, A. J., Turner, D. L., Reeves, G. D., Spence, H. E., Baker, D. N., & Blake, J. B. (2018). What causes radiation belt enhancements: A survey of the Van Allen probes era. *Geophysical Research Letters*, 45(11), 5253–5259. <https://doi.org/10.1029/2018gl077699>
- Brautigam, D. H., & Albert, J. M. (2000). Radial diffusion analysis of outer radiation belt electrons during the October 9, 1990, magnetic storm. *Journal of Geophysical Research*, 105(A1), 291–309. <https://doi.org/10.1029/1999ja900344>
- Bruno, A., Blum, L. W., de Nolfo, G. A., Kataoka, R., Torii, S., Greeley, A. D., et al. (2022). EMIC-wave driven electron precipitation observed by CALET on the international space station. *Geophysical Research Letters*, 49(6), e2021GL097529. <https://doi.org/10.1029/2021gl097529>
- Cao, X., Shprits, Y. Y., Ni, B., & Zhelavskaya, I. S. (2017). Scattering of ultra-relativistic electrons in the van Allen radiation belts accounting for hot plasma effects. *Scientific Reports*, 7(1), 17719. <https://doi.org/10.1038/s41598-017-17739-7>
- Capannolo, L., Li, W., Ma, Q., Chen, L., Shen, X.-C., Spence, H. E., et al. (2019). Direct observation of subrelativistic electron precipitation potentially driven by EMIC waves. *Geophysical Research Letters*, 46(22), 12711–12721. <https://doi.org/10.1029/2019gl084202>
- Carpenter, D. L., & Anderson, R. R. (1992). An ISEE/whistler model of equatorial electron density in the magnetosphere. *Journal of Geophysical Research Space Physics*, 97(A2), 1097–1108. <https://doi.org/10.1029/91JA01548>

- Chen, Y., Friedel, R. H. W., & Reeves, G. D. (2006). Phase space density distributions of energetic electrons in the outer radiation belt during two Geospace Environment Modeling Inner Magnetosphere/Storms selected storms. *Journal of Geophysical Research*, *111*(A11), A11S04. <https://doi.org/10.1029/2006JA011703>
- Da Silva, L. A., Shi, J., Alves, L. R., Sibeck, D., Souza, V. M., Marchezi, J. P., et al. (2021). Dynamic mechanisms associated with high-energy electron flux dropout in the Earth's outer radiation belt under the influence of a coronal mass ejection sheath region. *Journal of Geophysical Research: Space Physics*, *126*(1), e2020JA028492. <https://doi.org/10.1029/2020ja028492>
- Denton, R. E., Ofman, L., Shprits, Y. Y., Bortnik, J., Millan, R. M., Rodger, C. J., et al. (2019). Pitch angle scattering of sub-MeV relativistic electrons by electromagnetic ion cyclotron waves. *Journal of Geophysical Research Space Physics*, *124*(7), 5610–5626. <https://doi.org/10.1029/2018JA026384>
- Drozdov, A. Y. (2023). Replication data for: Distribution of seed electron phase space density minima in Earth's radiation belts [Dataset]. *UCLA Dataverse*. <https://doi.org/10.25346/S6/SDAVQ9>
- Drozdov, A. Y., Allison, H. J., Shprits, Y. Y., Elkington, S. R., & Aseev, N. A. (2021). A comparison of radial diffusion coefficients in 1-D and 3-D long-term radiation belt simulations. *Journal of Geophysical Research Space Physics*, *126*(8), e2020JA028707. <https://doi.org/10.1029/2020ja028707>
- Drozdov, A. Y., Allison, H. J., Shprits, Y. Y., Usanova, M. E., Saikin, A., & Wang, D. (2022). Depletions of multi-MeV electrons and their association to minima in phase space density. *Geophysical Research Letters*, *49*(8), e2021GL097620. <https://doi.org/10.1029/2021gl097620>
- Drozdov, A. Y., Shprits, Y. Y., Usanova, M. E., Aseev, N. A., Kellerman, A. C., & Zhu, H. (2017). EMIC wave parameterization in the long-term VERB code simulation. *Journal of Geophysical Research Space Physics*, *122*(8), 8501. <https://doi.org/10.1002/2017JA024389>
- Drozdov, A. Y., Usanova, M. E., Hudson, M. K., Allison, H. J., & Shprits, Y. Y. (2020). The role of hiss, chorus, and EMIC waves in the modeling of the dynamics of the multi-MeV radiation belt electrons. *Journal of Geophysical Research Space Physics*, *125*(9), 2628. <https://doi.org/10.1029/2020JA028282>
- Fukizawa, M., Sakanoi, T., Miyoshi, Y., Kazama, Y., Katoh, Y., Kasahara, Y., et al. (2022). Statistical study of approaching strong diffusion of low-energy electrons by chorus and ECH waves based on *in situ* observations. *Journal of Geophysical Research: Space Physics*, *127*(3), e2022JA030269. <https://doi.org/10.1029/2022ja030269>
- Green, J. C., & Kivelson, M. G. (2004). Relativistic electrons in the outer radiation belt: Differentiating between acceleration mechanisms. *Journal of Geophysical Research*, *109*(A3), A03213. <https://doi.org/10.1029/2003JA010153>
- Haas, B., Shprits, Y. Y., Allison, H. J., Wutzig, M., & Wang, D. (2023). A missing dusk-side loss process in the terrestrial electron ring current. *Scientific Reports*, *13*(1), 970. <https://doi.org/10.1038/s41598-023-28093-2>
- Hendry, A. T., Rodger, C. J., Chilverd, M. A., & Morley, S. K. (2021). Evidence of sub-MeV EMIC-driven trapped electron flux dropouts from GPS observations. *Geophysical Research Letters*, *48*(9), e2021GL092664. <https://doi.org/10.1029/2021gl092664>
- Hendry, A. T., Santolik, O., Kletzing, C. A., Rodger, C. J., Shiokawa, K., & Baishev, D. (2019). Multi-instrument observation of nonlinear EMIC-driven electron precipitation at sub-MeV energies. *Geophysical Research Letters*, *46*(13), 7248–7257. <https://doi.org/10.1029/2019GL082401>
- Horne, R. B., Thorne, R. M., Meredith, N. P., & Anderson, R. R. (2003). Diffuse auroral electron scattering by electron cyclotron harmonic and whistler mode waves during an isolated substorm. *Journal of Geophysical Research*, *108*(A7), 1290. <https://doi.org/10.1029/2002ja009736>
- Iles, R. H. A., Meredith, N. P., Fazakerley, A. N., & Horne, R. B. (2006). Phase space density analysis of the outer radiation belt energetic electron dynamics. *Journal of Geophysical Research*, *111*(A3), A03204. <https://doi.org/10.1029/2005JA011206>
- Kim, H., Schiller, Q., Engebretson, M. J., Noh, S., Kuzichev, I., Lanzerotti, L. J., et al. (2021). Observations of particle loss due to injection-associated electromagnetic ion cyclotron waves. *Journal of Geophysical Research Space Physics*, *126*(2), e2020JA029001. <https://doi.org/10.1029/2020ja028503>
- Li, W., Thorne, R. M., Ma, Q., Ni, B., Bortnik, J., Baker, D. N., et al. (2014). Radiation belt electron acceleration by chorus waves during the 17 March 2013 storm. *Journal of Geophysical Research Space Physics*, *119*(6), 4681–4693. <https://doi.org/10.1002/2014ja019945>
- Ma, X., Xiang, Z., Ni, B., Fu, S., Cao, X., Hua, M., et al. (2020). On the loss mechanisms of radiation belt electron dropouts during the 12 September 2014 geomagnetic storm. *Earth and Planetary Physics*, *4*(6), 1–13. <https://doi.org/10.26464/epp2020060>
- Malaspina, D. M., Jaynes, A. N., Boulé, C., Bortnik, J., Thaller, S. A., Ergun, R. E., et al. (2016). The distribution of plasmaspheric hiss wave power with respect to plasmopause location: PLASMAPAUSE-SORTED HISS. *Geophysical Research Letters*, *43*(15), 7878–7886. <https://doi.org/10.1002/2016GL069982>
- Malaspina, D. M., Ripoll, J.-F., Chu, X., Hospodarsky, G., & Wygant, J. (2018). Variation in plasmaspheric hiss wave power with plasma density. *Geophysical Research Letters*, *45*(18), 9417–9426. <https://doi.org/10.1029/2018GL078564>
- Malaspina, D. M., Zhu, H., & Drozdov, A. Y. (2020). A wave model and diffusion coefficients for plasmaspheric hiss parameterized by plasmopause location. *Journal of Geophysical Research Space Physics*, *125*(2), e2019JA027415. <https://doi.org/10.1029/2019JA027415>
- Millan, R. M., & Thorne, R. M. (2007). Review of radiation belt relativistic electron losses. *Journal of Atmospheric and Solar-Terrestrial Physics*, *69*(3), 362–377. <https://doi.org/10.1016/j.jastp.2006.06.019>
- Mozer, F. S., Agapitov, O. V., Hull, A., Lejosne, S., & Vasko, I. Y. (2017). Pulsating auroras produced by interactions of electrons and time domain structures. *Journal of Geophysical Research: Space Physics*, *122*(8), 8604–8616. <https://doi.org/10.1002/2017ja024223>
- Olifer, L., Mann, I. R., Ozeke, L. G., Morley, S. K., & Louis, H. L. (2021). On the formation of phantom electron phase space density peaks in single spacecraft radiation belt data. *Geophysical Research Letters*, *48*(11), e2020GL092351. <https://doi.org/10.1029/2020gl092351>
- Reeves, G. D., Spence, H. E., Henderson, M. G., Morley, S. K., Friedel, R. H. W., Funsten, H. O., et al. (2013). Electron acceleration in the heart of the Van Allen radiation belts. *Science*, *341*(6149), 991–994. <https://doi.org/10.1126/science.1237743>
- Rodger, C. J., Hendry, A. T., Chilverd, M. A., Kletzing, C. A., Brundell, J. B., & Reeves, G. D. (2015). High-resolution in-situ observations of electron precipitation-causing EMIC waves. *Geophysical Research Letters*, *42*(22), 9641. <https://doi.org/10.1002/2015GL066581>
- Saikin, A. A., Drozdov, A. Y., & Malaspina, D. M. (2022). Low frequency plasmaspheric hiss wave activity parameterized by plasmopause location: Models and simulations. *Journal of Geophysical Research Space Physics*, *127*(9), e2022JA030687. <https://doi.org/10.1029/2022ja030687>
- Shen, Y., Vasko, I. Y., Artemyev, A., Malaspina, D. M., Chu, X., Angelopoulos, V., & Zhang, X.-J. (2021). Realistic electron diffusion rates and lifetimes due to scattering by electron holes. *Journal of Geophysical Research: Space Physics*, *126*(9), e2021JA029380. <https://doi.org/10.1029/2021ja029380>
- Shprits, Y. Y., Drozdov, A. Y., Spasojevic, M., Kellerman, A. C., Usanova, M. E., Engebretson, M. J., et al. (2016). Wave-induced loss of ultra-relativistic electrons in the Van Allen radiation belts. *Nature Communications*, *7*(1), 12883. <https://doi.org/10.1038/ncomms12883>
- Shprits, Y. Y., Horne, R. B., Kellerman, A. C., & Drozdov, A. Y. (2018). The dynamics of Van Allen belts revisited. *Nature Physics*, *14*(2), 102–103. <https://doi.org/10.1038/nphys4350>
- Shprits, Y. Y., Kellerman, A., Aseev, N., Drozdov, A. Y., & Michaelis, I. (2017). Multi-MeV electron loss in the heart of the radiation belts. *Geophysical Research Letters*, *44*(3), 1209. <https://doi.org/10.1002/2016GL072258>

- Shprits, Y. Y., Kellerman, A. C., Drozdov, A. Y., Spence, H. E., Reeves, G. D., & Baker, D. N. (2015). Combined convective and diffusive simulations: VERB-4D comparison with 17 March 2013 Van Allen probes observations. *Geophysical Research Letters*, *42*(22), 9608. <https://doi.org/10.1002/2015GL065230>
- Shprits, Y. Y., Subbotin, D. A., Meredith, N. P., & Elkington, S. R. (2008). Review of modeling of losses and sources of relativistic electrons in the outer radiation belt II: Local acceleration and loss. *Journal of Atmospheric and Solar-Terrestrial Physics*, *70*(14), 1694–1713. <https://doi.org/10.1016/j.jastp.2008.06.014>
- Shprits, Y. Y., Thorne, R. M., Friedel, R., Reeves, G. D., Fennell, J., Baker, D. N., & Kanekal, S. G. (2006). Outward radial diffusion driven by losses at magnetopause. *Journal of Geophysical Research Space Physics*, *111*(A11), A11214. <https://doi.org/10.1029/2006JA011657>
- Shprits, Y. Y., Thorne, R. M., Reeves, G. D., & Friedel, R. (2005). Radial diffusion modeling with empirical lifetimes: Comparison with CRRES observations. *Annales Geophysicae*, *23*(4), 1467–1471. <https://doi.org/10.5194/angeo-23-1467-2005>
- Spasojevic, M., Shprits, Y. Y., & Orlova, K. (2015). Global empirical models of plasmaspheric hiss using Van Allen Probes. *Journal of Geophysical Research Space Physics*, *120*(12), 2015JA021803. <https://doi.org/10.1002/2015JA021803>
- Spence, H. E., Reeves, G. D., Baker, D. N., Blake, J. B., Bolton, M., Bourdarie, S., et al. (2013). Science goals and overview of the radiation belt storm probes (RBSP) energetic particle, composition, and thermal plasma (ECT) suite on NASA's Van Allen probes mission. *Space Science Reviews*, *179*(1), 311–336. <https://doi.org/10.1007/s11214-013-0007-5>
- Staples, F. A., Kellerman, A., Murphy, K. R., Rae, I. J., Sandhu, J. K., & Forsyth, C. (2022). Resolving magnetopause shadowing using multi-mission measurements of phase space density. *Journal of Geophysical Research Space Physics*, *127*(2), e2021JA029298. <https://doi.org/10.1029/2021JA029298>
- Subbotin, D. A., & Shprits, Y. Y. (2012). Three-dimensional radiation belt simulations in terms of adiabatic invariants using a single numerical grid. *Journal of Geophysical Research*, *117*(A5), A05205. <https://doi.org/10.1029/2011JA017467>
- Subbotin, D. A., Shprits, Y. Y., & Ni, B. (2011). Long-term radiation belt simulation with the VERB 3-D code: Comparison with CRRES observations. *Journal of Geophysical Research Space Physics*, *116*(A12), A12210. <https://doi.org/10.1029/2011JA017019>
- Summers, D., & Thorne, R. M. (2003). Relativistic electron pitch-angle scattering by electromagnetic ion cyclotron waves during geomagnetic storms. *Journal of Geophysical Research Space Physics*, *108*(A4), 1143. <https://doi.org/10.1029/2002JA009489>
- Thorne, R. M., Li, W., Ni, B., Ma, Q., Bortnik, J., Chen, L., et al. (2013). Rapid local acceleration of relativistic radiation-belt electrons by magnetospheric chorus. *Nature*, *504*(7480), 411–414. <https://doi.org/10.1038/nature12889>
- Tsyganenko, N. A. (1989). A magnetospheric magnetic field model with a warped tail current sheet. *Planetary and Space Science*, *37*(1), 5–20. [https://doi.org/10.1016/0032-0633\(89\)90066-4](https://doi.org/10.1016/0032-0633(89)90066-4)
- Turner, D. L., Angelopoulos, V., Shprits, Y., Kellerman, A., Cruce, P., & Larson, D. (2012). Radial distributions of equatorial phase space density for outer radiation belt electrons. *Geophysical Research Letters*, *39*(9), 9101. <https://doi.org/10.1029/2012GL051722>
- Turner, D. L., O'Brien, T. P., Fennell, J. F., Claudepierre, S. G., Blake, J. B., Jaynes, A. N., et al. (2017). Investigating the source of near-relativistic and relativistic electrons in Earth's inner radiation belt. *Journal of Geophysical Research Space Physics*, *122*(1), 695–710. <https://doi.org/10.1002/2016JA023600>
- Turner, D. L., Shprits, Y., Hartinger, M., & Angelopoulos, V. (2012). Explaining sudden losses of outer radiation belt electrons during geomagnetic storms. *Nature Physics*, *8*(3), 208–212. <https://doi.org/10.1038/nphys2185>
- Ukhorskiy, A. Y., Shprits, Y. Y., Anderson, B. J., Takahashi, K., & Thorne, R. M. (2010). Rapid scattering of radiation belt electrons by storm-time EMIC waves. *Geophysical Research Letters*, *37*(9), L09101. <https://doi.org/10.1029/2010GL042906>
- Usanova, M. E., Drozdov, A., Orlova, K., Mann, I. R., Shprits, Y., Robertson, M. T., et al. (2014). Effect of EMIC waves on relativistic and ultrarelativistic electron populations: Ground-based and Van Allen Probes observations. *Geophysical Research Letters*, *41*(5), 1375–1381. <https://doi.org/10.1002/2013GL059024>
- Vasko, I. Y., Agapitov, O. V., Mozer, F. S., Artemyev, A. V., Krasnoselskikh, V. V., & Bonnell, J. W. (2017). Diffusive scattering of electrons by electron holes around injection fronts. *Journal of Geophysical Research Space Physics*, *122*(3), 3182. <https://doi.org/10.1002/2016JA023337>
- Wu, H., Chen, T., Kalegaev, V. V., Panasyuk, M. I., Vlasova, N. A., Duan, S., et al. (2020). Long-term dropout of relativistic electrons in the outer radiation belt during two sequential geomagnetic storms. *Journal of Geophysical Research: Space Physics*, *125*(10), e2020JA028282. <https://doi.org/10.1029/2020ja028098>
- Xiang, Z., Tu, W., Li, X., Ni, B., Morley, S. K., & Baker, D. N. (2017). Understanding the mechanisms of radiation belt dropouts observed by Van Allen Probes. *Journal of Geophysical Research: Space Physics*, *122*(10), 9183. <https://doi.org/10.1002/2017JA024487>
- Xiong, Y., Xie, L., Fu, S., Ni, B., & Pu, Z. (2021). Non-storm erosion of MeV electron outer radiation belt down to $L^* < 4.0$ associated with successive enhancements of solar wind density. *Earth and Planetary Physics*, *5*(5), 1–11. <https://doi.org/10.26464/epp2021051>
- Yan, Y., Yue, C., Ma, Q., Zhou, X.-Z., Zong, Q.-G., Fu, H., et al. (2023). Prompt appearance of large-amplitude EMIC waves induced by solar wind dynamic pressure enhancement and the subsequent relativistic electron precipitation. *Journal of Geophysical Research: Space Physics*, *128*(7), e2023JA031399. <https://doi.org/10.1029/2023ja031399>
- Zhao, H., Baker, D. N., Li, X., Malaspina, D. M., Jaynes, A. N., & Kanekal, S. G. (2019). On the acceleration mechanism of ultrarelativistic electrons in the center of the outer radiation belt: A statistical study. *Journal of Geophysical Research: Space Physics*, *124*(11), 8590–8599. <https://doi.org/10.1029/2019ja027111>
- Zhu, H., Shprits, Y. Y., Spasojevic, M., & Drozdov, A. Y. (2019). New hiss and chorus waves diffusion coefficient parameterizations from the Van Allen Probes and their effect on long-term relativistic electron radiation-belt VERB simulations. *Journal of Atmospheric and Solar-Terrestrial Physics*, *193*, 105090. <https://doi.org/10.1016/j.jastp.2019.105090>